Contributions to Mineralogy and Petrology (2020) 175:38
https://doi.org/10.1007/s00410-020-01676-2

ORIGINAL PAPER

Discontinuous precipitation of rutilated quartz: grain-boundary migration induced by changes to the equilibrium solubility of Ti in quartz

Jay B. Thomas[1] · William O. Nachlas[1]

Published online: 2 April 2020

Abstract
We experimentally investigated changes to the titanium concentrations of quartz-rich rocks caused by grain-boundary migration. Synthesis experiments were performed to make high-Ti quartz starting materials for usage in recrystallization experiments. We isothermally recrystallized quartz starting material in separate experiments at 10–25 kbar to reduce the solubility of Ti in quartz. Microstructural and geochemical results indicate that the high-Ti quartz starting material recrystallized to form low-Ti quartz with acicular rutile inclusions. During recrystallization, high-Ti quartz was consumed to form low-Ti quartz and acicular rutile crystals precipitated behind moving grain boundaries via the discontinuous precipitation unmixing process. Experimentally imposed changes to the equilibrium solubility concentration of Ti in quartz by amounts as low as ~ 0.02 weight % (200 µg/g or ppm by weight) created a free energy driving force of 8.7 kJ/mol that was sufficient to drive large-scale recrystallization of the quartzites. Microstructures of relict grains of the high-Ti quartz starting materials are characterized by cuspate and irregular grain boundaries, whereas new quartz grains exhibit subhedral to euhedral grain morphologies and abundant three-grain junctions. Discontinuous precipitation can significantly change mineral compositions, and in the absence of a free fluid phase can operate much faster than other types of mass transfer processes commonly associated with solid-state reactions.

Keywords Quartz · Rutile · Grain boundary migration · Discontinuous precipitation · Rutilated quartz

Introduction

Quartz-quartz grain boundaries are among the most abundant interfaces in the Earth's continental lithosphere. Given the abundance of quartz in igneous, metamorphic, and sedimentary rocks, combined with its propensity to accommodate deformation through various grain size-reducing processes, the grain-boundary regions separating adjacent quartz crystals in rocks exert first-order controls on a wide range of geochemical, petrologic, geophysical, and geodynamic processes. Grain boundaries are < 1 nm wide regions separating crystals with different orientations. Kinetic feedback mechanisms that operate along grain boundaries strongly control the compositional and textural properties of rocks (e.g., Thomas and Watson 2014). Grain boundaries are important geochemical reservoirs of elements that are not compatible in the dominant matrix minerals of polycrystalline materials (Hiraga et al. 2002, 2007; Hiraga and Kohlstedt 2007), and grain-boundary diffusion mediates transport of elements in systems that lack a wetting fluid or melt (Thomas and Watson 2014; Bromiley and Hiscock 2016). Partitioning of elements into static grain-boundary regions and subsequent grain-boundary transport exert strong controls on elemental and isotopic fractionations (Farver and Yund 1992; Teng et al. 2006; Tominaga et al. 2009), and mineral nucleation and growth (Thomas and Watson 2014).

In polycrystalline rocks lacking a wetting fluid or melt, grain boundaries are the only geometric pathway for coexisting minerals to "communicate" with one another in response to changes in *P*–*T*–*X* conditions. Metamorphic reactions that operate by moving grain boundaries through rocks can govern textural development and significantly modify mineral geochemistry. Migration of grain

Communicated by Mark S Ghiorso.

✉ Jay B. Thomas
jthom102@syr.edu

[1] 204 Heroy Geology Laboratory, Department of Earth Sciences, Syracuse University, Syracuse, NY 13244, USA

boundaries occurs as ions change their position between neighboring crystals, which causes relative motion of the interfaces separating adjacent grains. Moving grain-boundary reactions that involve changes to mineral chemistry of adjacent crystals are called discontinuous reactions because the moving grain boundary produced a structural (i.e., orientation) and chemical discontinuity between the reactant and product minerals formed behind the moving interface (Boland and van Roermund 1983; Boland and Otten 1985; Putnis 1992; Manna et al. 2001). Discontinuous precipitation (DP) is fundamentally different from other moving interface reactions (e.g., spinodal decomposition, diffusion-induced or chemically induced grain-boundary migration, and diffusion-induced recrystallization) because DP involves decomposing a supersaturated solid solution into two new minerals that precipitate at a moving grain boundary. Numerous studies document DP reactions in natural (Nichols et al. 2018) and engineered metallic systems (Manna et al. 2001), and DP reactions can produce symplectite textures in silicate rocks (Boland and van Roermund 1983; Boland and Otten 1985). We argue that DP reactions are a mechanism to produce finely rutilated quartz and may play an important role in the development of quartz microstructures. Quartz with acicular needles forms instead of lamellar symplectites of quartz and coarser-grained rutile likely because changes to Ti concentrations of quartz occur at trace element levels—the maximum change produced here was ~ 200 ppm Ti (TiO_2 mole fraction = 2.7×10^{-4}). In contrast, for example, the generic symplectite-producing reaction common to eclogites is diopside + albite = 2omphacite + quartz.

Previous experimental studies showed that grain boundary migration under hydrostatic (Thomas et al. 2015) and deformation (Nachlas et al. 2018a) conditions can modify Ti concentrations of quartz, but DP reactions were not fully appreciated. Here we present new piston-cylinder experiments to explore reactions that operated along moving grain boundaries in synthesized quartzites. We made high-Ti quartz for usage as starting material. The quartz starting material was recrystallized in separate experiments at 10–25 kbar to reduce Ti solubility. Light microscopy, cathodoluminescence, field-emission scanning electron microscopy, electron probe microanalysis, and electron backscattered diffraction measurements were used to characterize experimental run products. Light microscopy unequivocally revealed DP of finely rutilated quartz that formed behind moving grain boundaries. We used a Ti-in-quartz solubility model to determine the magnitudes of chemical driving forces that caused grain-boundary migration and discontinuous precipitation. Results demonstrate that DP in quartzites operates in response to trace-level impurity differences between neighboring grains. The length scales of chemical and textural modifications caused by DP are compared to geochemical changes caused by some other mass transfer processes (e.g., volume diffusion, grain-boundary diffusion).

Experimental and analytical methods

We performed two types of high *P–T* experiments using end-loaded piston-cylinder devices at Syracuse University and Rensselaer Polytechnic Institute. *Synthesis experiments* were performed to make high-Ti quartz starting materials for usage in *recrystallization experiments*. Both types of experiments used Ag capsules contained in NaCl-Pyrex-MgO assemblies wrapped in Pb foil (Watson et al. 2002). Experiments performed at $P < 20$ kbar used 19 mm diameter assemblies and experiments performed at $P \geq 20$ kbar used 12.7 mm diameter assemblies. The piston-cylinder devices employed Enerpac Bourdon tube gauges with 18 cm-diameter dials to measure hydraulic oil pressures. Temperatures were controlled to ± 1 °C using type-D thermocouples ($W_{97}Re_3$–$W_{75}Re_{25}$) and Eurotherm Nanodac PID controllers (thermocouple accuracy reported from Concept Alloys is ± 0.5 °C). We did not apply "friction corrections" to the calculated experimental pressures because reported pressures are interpreted as accurate to within approximately ± 120 bars (Spear et al. 2014; Thomas and Spear 2018; Bonazzi et al. 2019). Shutting off power to the assemblies quenched experiments to below 100 °C in less than 30 s.

Quartz starting materials were synthesized from hydrothermal fluids in the SiO_2-ZrO_2-TiO_2 system at 10 kbar and 925 °C. Oxide starting materials (Alfa Aesar) consisted of SiO_2 (amorphous; ~ 40 mg), TiO_2 (anatase; ~ 5 mg), ZrO_2 (~ 5–10 mg), and water (distilled or deionized; ~ 25 mg). Powders were gently loaded into silver capsules with ~ 1 mm-thick walls and water was added to fill capsules to within ~ 1 mm of the lid (Thomas et al. 2015). Experimental capsules were sealed during cold pressurization at room temperature.

We opened synthesis experiment capsules with two pairs of pliers by wrenching off capsule lids. Crystals were washed out of capsules with alcohol or water. After drying, we handpicked single crystals from the synthesis experiments, placed them on double-sided tape, and cast them in epoxy. The remaining high-Ti quartz starting materials were hammered into Ag capsules using a drill blank to pulverize the material. After recrystallization experiments, we machined off the majority of capsule lids and bottoms using a lathe to expose fully densified polycrystalline rocks. Recrystallization experiments were vacuum impregnated and cast in epoxy.

All experimental specimens were ground flat with silicon carbide papers (600 grit), polished in 1 µm alumina, and final polished for 2 h in 60 nm colloidal silica suspensions,

which produced a featureless finish suitable for subsequent analyses. We polished both sides of some specimens for transmitted light microscopy and confocal Raman microprobe measurements.

The Cameca SXFive electron probe microanalyzer (EPMA) at Syracuse University and the Cameca SX100 microprobe at Rensselaer Polytechnic Institute were used for trace element measurements of titanium in quartz. Both instruments have cathodoluminescence (CL) imaging capabilities used to document Ti distribution in experimental run products; CL imaging was performed using 10 to 100 nA beam currents and 15 kV accelerating voltage. For quantitative measurements, the five wavelength dispersive spectrometers were tuned, and elements were standardized using oxide and silicate mineral standards by adjusting the beam current to attain ~ 12,000 counts per second for analyte X-rays on gas-flow proportional counters. Trace element measurements of Ti in quartz were performed using a 200 nA beam current and a "focused" beam (< 1 µm diameter). Titanium Kα X-rays were diffracted with large PET diffraction crystals (22 × 60 mm) and simultaneously counted on four spectrometers (200 s on peak, and 100 s on low and high backgrounds), which yielded a statistical detection limit between 5 and 8 ppm (by weight) for individual measurements. We counted Si Kβ X-rays to confirm analyzed materials were silica and for accurate matrix correction. We evaluated accuracy of EPMA measurements by analyzing quartz reference materials including synthetic quartz reference materials from Thomas et al. (2010) with 18–813 ppm Ti. It was not possible to completely avoid rutile crystals contained in the recrystallized experiments, so not all recrystallization experiments were measured with EPMA.

We measured the crystallographic orientations of quartz in polycrystalline quartzites produced in recrystallization experiments using electron backscatter diffraction (EBSD) with a Tescan Vega3 scanning electron microscope with Oxford EBSD detector housed at the State University of New York (New Paltz). The experimental sample was tilted at 70° to the incident beam and analyzed at 18 mm working distance with a 25 kV, ~ 12 nA electron beam. We collected EBSD maps of 201,000 to 276,000 µm^2 areas using a 1 µm step size. Regions selected for mapping contained mostly quartz, and greater than 90% of the pixels indexed as quartz, rutile, or zircon. Crystallographic orientation data were processed and analyzed using the open-source MTEX module for MATLAB (Bachmann et al. 2010). Individual grains were defined as regions separated by > 10° (Shigematsu et al. 2006) that contain at least 8 pixels. Dauphine twins (60° rotation about α quartz c axis) were identified in both relict and recrystallized quartz.

Field emission scanning electron microscopes at Rensselaer Polytechnic Institute (Carl Zeiss Crossbeam) and Cornell University (Carl Zeiss Gemini) were used to image recrystallization experiments. Secondary and backscattered electron images were acquired using 20 kV accelerating voltage. X-ray analyses were performed using an Oxford AZTEC energy dispersive spectrometer.

Raman spectra of experimental run products were measured with a Renishaw In-Via Raman microprobe at Syracuse University. The incident laser light (532 nm) was focused onto targets using a 100X objective (N.A. = 0.9). We performed depth profiles through acicular mineral inclusions that are < 1 µm wide by moving the motorized stage in 0.3 µm increments. Spectra were acquired for 20 s. Raman shifted light was backscattered (180° geometry) and statically dispersed with 1800 grooves/mm gratings onto a charged-couple device. The Renishaw spectrometer has ~ 0.5 cm^{-1} spectral resolution (dependent on wavelength of shifted light), and precision of standard measurements is typically < 0.1 cm^{-1}. The spectrometer was calibrated against numerous Ne lines, and spectral accuracy and linearity were checked throughout each analytical session by measuring the Rayleigh scattered laser light and the 520.5 cm^{-1} band of a silicon standard.

Results

One of the examined recrystallization experiments is from a previous study (Thomas et al. 2015) deployed to evaluate the *P–T* dependencies of the Ti-in-quartz solubility models used in thermobarometry. In that study, high-Ti quartz was recrystallized under "wet" and "dry" conditions. Based on results from reflected light microscopy, CL, and EPMA, Thomas et al. (2015) suggested that quartz crystals in dry experiments recrystallized via chemically induced grain-boundary migration. All results of the previous study were from polished sections of experimental capsules (i.e., the capsule bottoms remained). After completion of the Thomas et al. (2015) study, we cut off the bottoms of the capsules to prepare sections polished on both sides to permit transmitted light microscopy. We then discovered that the recrystallized quartz in "dry" experiments contain numerous acicular rutile inclusions with < 1 µm diameters that were not previously recognized. Chemically induced grain-boundary migration and DP are related discontinuous reactions, but the presence of the rutile crystals locally precipitated in the "wake" of moving grain boundaries indicates that the microstructures technically formed by DP. Identification of the acicular rutile crystals that developed in the dry recrystallization experiments motivated additional experiments described here.

Synthesis experiments to make high-Ti quartz

The generic reaction,

$$TiO_2^{quartz} \overset{P,T}{\leftrightarrow} TiO_2^{rutile} \quad (1)$$

describing the equilibrium solubility of Ti^{4+} contained in the quartz structure and the solubility model of Thomas et al. (2010) were used to guide synthesis experiments and to study quartz recrystallization processes under nominally dry conditions. Experimental run conditions and Ti concentrations of synthesis and recrystallization experiments are shown in Fig. 1 and listed in Table 1. As briefly described above, synthesis experiments conducted at 925 °C and 10 kbar were performed to make the quartz starting material. Aqueous fluid was always present after opening synthesis capsules. Each synthesis experiment produced thousands of anhedral to euhedral quartz crystals that ranged up to ~ 1 mm in diameter, and granular rutile and zircon with lengths typically < 100 µm and length/width aspect ratios ~ 2. Raman spectroscopy confirmed that the starting oxide powders crystallized to form quartz, rutile, and zircon during the synthesis experiments (Fig. 2). Transmitted light microscopy revealed that most quartz crystals from the synthesis experiments are free of inclusions, but some crystals contain inclusions of primary rutile and zircon; fluid inclusions occur but are rare. Cathodoluminescence images with uniform brightness values and EPMA measurements of quartz crystals demonstrate that Ti concentrations in quartz are relatively uniform; synthesized quartz starting material contained ~ 349 to 392 ppm Ti (see estimated standard deviations in Table 1). Titanium concentrations of synthesized quartz starting material (Fig. 1) are within the 95% confidence interval of the Ti-in-quartz solubility model of Thomas et al. (2010). The reproducibility of Ti concentrations in quartz grown in numerous experiments using five different piston-cylinder devices located at two universities is noteworthy (Table 1; Wark and Watson 2006; Thomas et al. 2010, 2015).

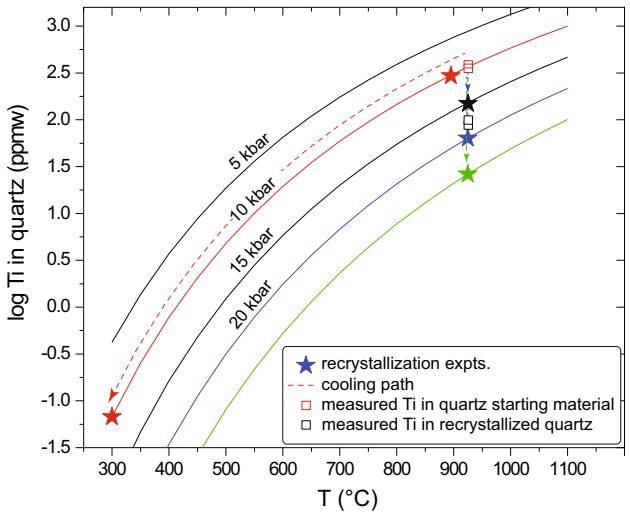

Fig. 1 Plot showing the pressure and temperature dependencies of Ti in quartz. Curves are the Ti-in-quartz solubility model of Thomas et al. (2010). The recrystallization experiment at 10 kbar is offset from 925 °C to avoid overlapping the measured Ti in quartz of synthesized quartz starting materials. Errors (two standard errors) are smaller than the symbols. The dashed line shows a cooling experiment. See text for details

Recrystallization experiments

It was not possible to remove all rutile and zircon from the quartz starting material used in recrystallization experiments. We forcibly hammered the quartz starting material into new capsules for the recrystallization experiments (see Methods) to reduce porosity and pulverize the starting material. No water was added to capsules. We performed recrystallization experiments in 5 kbar increments along the 925 °C isotherm from the synthesis condition at 10 kbar up to 25 kbar (Fig. 1; Table 1). We also performed a cooling

Table 1 Experimental run conditions and Ti concentrations of quartz

Name	*P* (kbar)	*T* (°C)	*t* (h)	H2O (wt%)	Measured Ti (ppm)	Calculated Ti (ppm)
Synthesis experiments						
QTiP-43	10	925	98.7	40	392 (2)	367
QTiP-44	10	925	120	45	349 (50)	367
QTiP-47	10	925	120	45	376 (26)	367
Recrystallization experiments						
TiiGrB-21	10	925	120	0	nd	367
TiiGrB-17	10	925–300	*18.3 + 173.6	0	nd	367–0.1
TiiGrB-20	15	925	120	0	nd	153
TiiGrB-1	20	925	120	0	100 (2)	84
TiiGrB-18	25	925	120	0	nd	27

1. Experiments QTiP-43 and TiiGrB-1 are from Thomas et al. (2015); numbers in parentheses are estimated 2 s. *TiiGrB-17 dwelled for 18.3 h at 925 °C prior to ramping down temperature to 300 °C

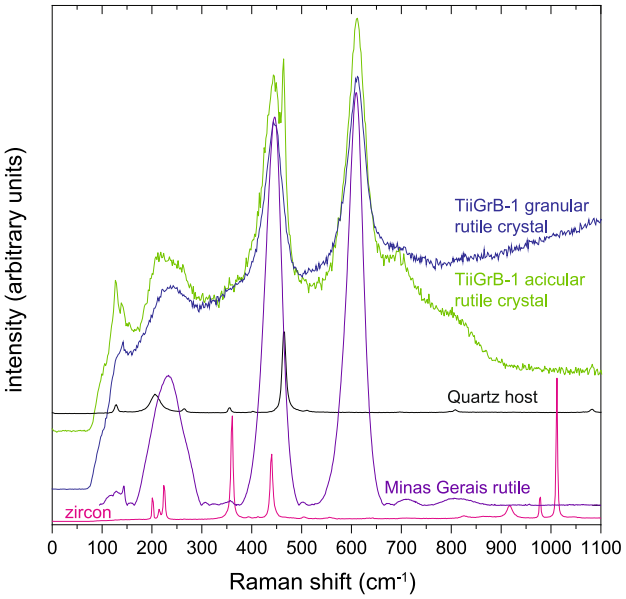

Fig. 2 Raman spectra of quartz, rutile, and zircon from recrystallization experiment TiiGrB-1 that exhibits decomposition of high-Ti quartz by discontinuous precipitation of low-Ti quartz and acicular rutile. A spectrum of rutile (Minas Gerais, Brazil) for reference is from the RRUFF database (Lafuente et al. 2015)

experiment along the 10 kbar isobar with the goal of homogeneously precipitating rutile from high-Ti quartz.

Cathodoluminescence textures of recrystallization experiments

Textural evidence that reactions operating along moving grain boundaries modified Ti concentrations in quartzites was first described in natural samples by Müller et al. (2007) and later experimentally demonstrated by Thomas et al. (2015) and Nachlas et al. (2018a) based on CL images of quartzites recrystallized under isostatic and dynamic conditions, respectively. CL brightness directly correlates with variations in Ti concentrations in quartz (Spear et al. 2012), making CL an especially useful method for evaluating modifications to quartz Ti concentrations during recrystallization. Because the induced compositional variations are present at trace element levels, other commonly used observational methods cannot directly reveal the extent of recrystallization (e.g., reflected light microscopy and other types of scanning electron microscopy). Importantly, CL imaging is always the initial reconnaissance method used to evaluate recrystallization because cutting off capsule bottoms, grinding, and polishing experimental capsules containing polycrystalline aggregates sufficiently thin for light transmission (< 100 µm) removes valuable material and risks destroying experimental specimens.

A recrystallization experiment performed at the same *P–T* condition as the synthesis experiment (10 kbar and 925 °C), which is regarded as a null experiment, produced a polycrystalline aggregate composed of angular fragments of pulverized quartz starting material with relatively uniform CL brightness (Fig. 3a). Aside from some healed fractures in quartz starting material, textural evidence for substantial microstructure modification is absent. Titanium concentrations of quartz crystals are essentially identical to the quartz starting material (Table 1).

Cathodoluminescence images show that quartz in all recrystallization experiments conducted at $P > 10$ kbar underwent extensive recrystallization. The polycrystalline quartzites have equilibrium microstructures with equant quartz crystals joined at ~ 120° triple-grain junctions (Figs. 3b, c, 4a, b). There is no textural evidence indicating the presence of a free fluid phase during experiments (e.g., wetted triple junctions, grain boundaries, etc.), and fluid inclusions do not occur in any of the recrystallized grains. CL images and EPMA measurements demonstrate that quartz grown in the recrystallization experiments has substantially lower Ti concentrations than the quartz starting material (Fig. 4a; Thomas et al. 2015), consistent with solubility models that predict reduced Ti concentration with increasing pressure (Fig. 1; Table 1; Thomas et al. 2010, 2015).

The recrystallized quartz crystals have dark CL and well-developed facets that directly impinge on the high-Ti quartz starting material (bright CL; Fig. 4a). For this reason, the high-Ti quartz always occurs as individual grains with bright CL and cuspate grain boundaries. The high-Ti quartz starting material never occurs as cores with crystallographically continuous overgrowths of dark-CL quartz, which is a common texture that occurs in "wet" quartzite recrystallization experiments described in Thomas et al. (2015) that were interpreted to have recrystallized by dissolution–precipitation processes. Based on interpretations of EBSD results described below, many of the recrystallized regions shown in Fig. 3b were likely large single crystals of high-Ti quartz starting material that were replaced (partially or completely; Fig. 3b, c) by numerous smaller quartz crystals to form an equilibrium microstructure of equant grains with similar dimensions. We emphasize that significant microstructural development was not observed in the null experiment recrystallized at the synthesis condition.

Nucleation of the new quartz grains in the quartzites is not well understood, but we speculate that nucleation occurred within high-energy regions of the quartz starting material followed by radial growth outwards. Some recrystallized quartz crystals display fine-scale chemical zonation, indicating that attainment of chemical equilibrium by grain-boundary migration may have been incomplete (cf. Manna et al. 2001).

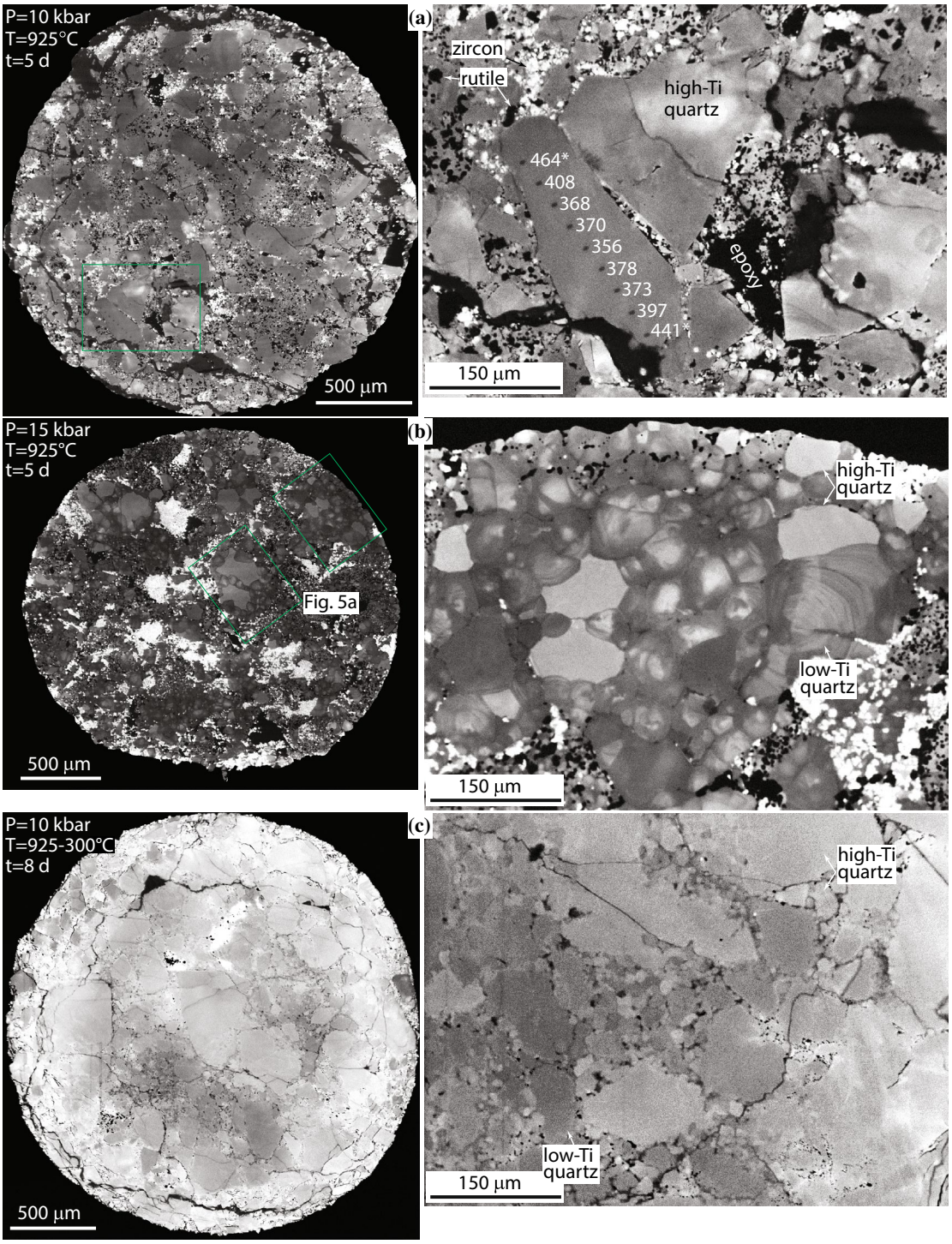

Fig. 3 Cathodoluminescence images of recrystallization experiment capsule cross-sections (left) and higher magnification images of microstructures (right). **a** A "null" recrystallization experiment performed at the same *P–T* conditions as the synthesis experiment used to make the starting material (TiiGrB-21; Table 1). Note that quartz crystals remain as angular fragments with unaltered Ti concentrations. Titanium concentrations near the ends of the crystal with asterisks were affected by secondary fluorescence from nearby rutile. **b** Recrystallization experiment performed at 15 kbar and 925 °C (TiiGrB-20; Table 1). Most high-Ti quartz starting material was consumed in the discontinuous reaction high-Ti quartz = low-Ti quartz + rutile. The high-Ti quartz has irregular cuspate boundaries impinged by low-Ti quartz. Concentric zoning of the low-Ti quartz indicates that imperfect chemical equilibrium was achieved during the recrystallization experiment. **c** Isobaric slow cooling experiment (TiiGrB-17; Table 1). High-Ti quartz has serrated and irregular grain boundaries; the newly formed quartz with dark-CL forms a finer-grained microstructure compared to the isothermal experiments performed at higher temperatures, and evidence for grain migration in the form of cuspate boundaries or triple junctions is absent

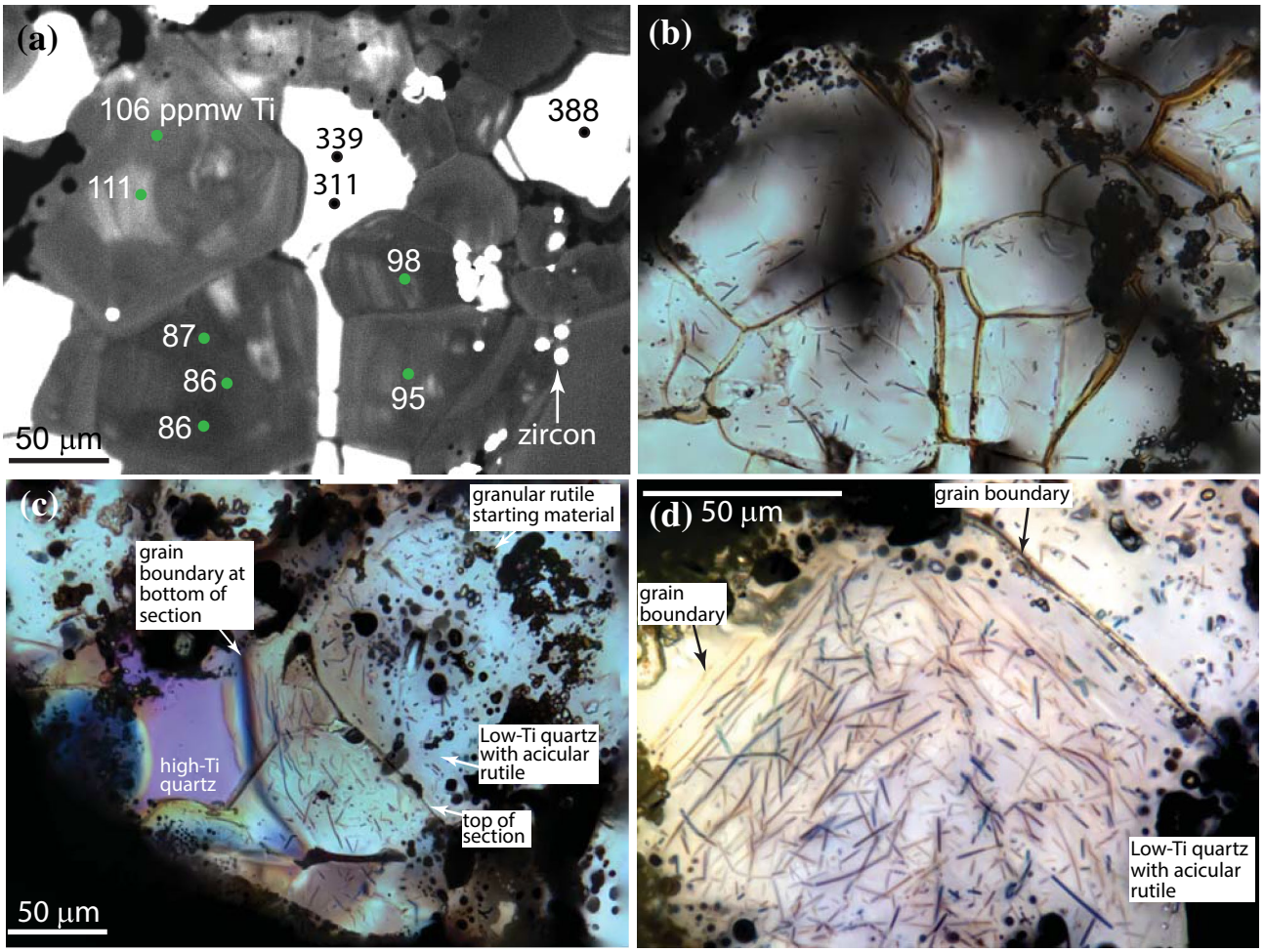

Fig. 4 Images of recrystallization experiment performed at 20 kbar and 925 °C (TiiGrB-1; Table 1). Cathodoluminescence image **a** and the corresponding transmitted plane-polarized light photomicrograph Field of view=312 micrometers. **b** showing that high-Ti quartz recrystallized to produce low-Ti quartz with dark-CL and acicular rutile crystals. Crossed polarized **c** and plane-polarized transmitted light photomicrographs **d** are composites of 18 stacked photographs taken throughout a 90-μm-thick section of the recrystallization experiment. Note the acicular rutile crystals that trace the exterior crystal shape of quartz near center of photograph (**c**)

We ran a cooling experiment (3.6 °C/h) along the 10 kbar isobar (Fig. 1) to evaluate textural changes that result from decreased Ti-in-quartz solubility in response to decreasing temperature. Because cooling was relatively rapid, recrystallization was considerably more limited than previous recrystallization experiments and restricted to irregular, serrated quartz-quartz boundaries characterized by dark-CL recrystallized quartz adjacent to high-Ti relict quartz crystals (Fig. 3c). The serrated grain boundaries resemble grain-boundary bulge recrystallization textures (Urai et al. 1986; Hirth and Tullis 1992). Relative to the isothermal experiments, quartz in the cooling experiment experienced more limited textural and chemical modifications likely related to decreased grain-boundary migration rates with decreasing temperature.

It was nearly impossible to obtain accurate Ti measurements of dark-CL, recrystallized quartz because of pervasive secondary fluorescence from abundant acicular rutile inclusions formed during recrystallization experiments (see below) as well as granular rutile crystals included with the starting material (Fig. 4b–d). Recrystallized quartz grains with dark CL (Fig. 4a) that have Ti concentrations close to the equilibrium solubility (Fig. 1) occur in isolated regions that do not contain many nearby acicular rutile crystals (Fig. 4b). Titanium concentrations in doubly polished thin (< 30 μm) crystals of dark-CL quartz (Fig. 4a) from the experiment at 20 kbar and 925 °C range from 86 to 113 ppm Ti and have an average of 100 ppm Ti (Fig. 1; Table 1). Secondary fluorescence from abundant rutile inclusions in recrystallized quartz produces Ti concentrations in all recrystallization experiments (Thomas et al. 2015) that are slightly higher than predicted by the Ti-in-quartz solubility model (Fig. 1).

Titanium depletion haloes surrounding rutile inclusions in quartz were observed in CL images of some natural rutilated quartz crystals (Cherniak et al. 2007; Nachlas et al.

2018b). We do not observe any CL variation in quartz surrounding rutile crystals in these experimental specimens.

Transmitted light microscopy of recrystallization experiments

At the time when the recrystallization experiments of Thomas et al. (2015) were measured, we did not know that the recrystallized quartz was thoroughly rutilated because we had not observed experimental specimens in transmitted light. Thomas et al (2015) attributed relatively large ranges of Ti concentrations measured in the recrystallized dark-CL quartz to secondary fluorescence analytical artifacts caused by nearby/subsurface granular rutile crystals that were inadvertently added from the original synthesis experiments (Fig. 4b–d). The acicular rutile crystals were not visible with reflected light microscopy typically used to examine polished samples of experimental specimens. The acicular crystals were also not resolvable with backscattered and secondary electron imaging obtained using the LaB_6 and tungsten filament electron sources in our EPMA and SEM-EBSD instruments, respectively.

Transmitted light microscopy revealed that the interiors of recrystallized grains with dark CL are thoroughly rutilated. Acicular rutile crystals are remarkably well resolved at high magnification in transmitted light with a petrographic microscope (Fig. 4b–d), likely because many rutile crystals have width dimensions (i.e., equivalent a- and b-axes in tetragonal rutile) near the wavelengths of transmitted visible light (i.e., ~ 380–780 nm) (Seifert et al. 2011). Transmitted light and CL images in Fig. 4a–d show that relict grains of high-Ti quartz with bright CL never contain acicular rutile crystals, whereas recrystallized low-Ti quartz with dark CL always contains acicular rutile crystals. Transmitted light microscopy also revealed that dark-CL quartz in restricted regions (e.g., Fig. 4a) have Ti concentrations approaching predicted equilibrium values because quartz crystals in those regions are very thin and contain few acicular rutile crystals (Fig. 4b).

The acicular rutile crystals that formed during the recrystallization experiments may be aligned at angles to or along the lengths of quartz grain boundaries (Fig. 4c). Petrographic observations indicate that acicular rutile crystals have high aspect ratio with long axes typically > 100 μm and widths always < 1 μm (Fig. 4b–d). Many acicular rutile crystals apparently delineate positions of a former grain boundary as the new quartz crystal grain boundary migrated to consume the out-of-equilibrium quartz with high Ti concentrations (Fig. 4c, d). Some acicular rutile crystals are curved and trace former facets developed on migrating quartz grain boundaries (see Fig. 4c). The acicular rutile crystals are not correlated with quartz symmetry presumably because some rutile crystals nucleated at random angles to the migrating grain boundaries, and because not all new quartz crystals are perfectly faceted.

The quartz in water-saturated recrystallization experiments of Thomas et al. (2015) has bright-CL quartz with overgrowth mantles of dark-CL quartz with low Ti concentrations. Based on CL textural relationships, Thomas et al. concluded that the high-Ti quartz starting material in the water-saturated experiments recrystallized by dissolution–precipitation processes to produce low-Ti rims that contained the equilibrium solubility concentration of Ti. Titanium that exceeded the equilibrium solubility concentration during recrystallization must have been partitioned into fluid along the grain boundaries and subsequently transported to preexisting rutile crystals residing on grain boundaries. Notably, quartz recrystallized in the water-saturated experiments do not contain acicular rutile crystals.

Electron backscatter diffraction measurements of recrystallization experiments

We used EBSD to measure crystallographic orientations of quartz in the recrystallization experiments. Goals of EBSD measurements were to evaluate intracrystalline structure and determine misorientation along boundaries between relict high-Ti quartz crystals and low-Ti quartz that formed during the recrystallization experiments. EBSD maps reveal large, single crystals of relict quartz mantled by multiple smaller, equant grains of recrystallized low-Ti quartz (Fig. 5a–c). The EBSD maps also clearly show that recrystallized quartz formed a foam-like texture characteristic of an equilibrium microstructure at the expense of the high-Ti quartz. Most of the mapped region shown in Fig. 5 was likely one large single crystal of high-Ti quartz surrounded by fine-grained rutile and zircon. The EBSD maps also suggest that recrystallized quartz crystals may have nucleated along a fracture near the center of the relict high-Ti quartz crystal (Fig. 5a–c) followed by outward growth. The radius of grain-boundary curvature of recrystallized grains points from crystal nuclei outwards in the growth direction. Recrystallized quartz crystals do not exhibit preferred orientations, and they show no evidence for intracrystalline distortion (cf. Nachlas et al. 2018a). The high-Ti relict grains and the numerous low-Ti recrystallized grains do not exhibit preferred misorientations along shared boundaries, suggesting that grain misorientation was not a major driving force for grain-boundary migration in these experiments (Fig. 5b). Dauphiné twins occur in both relict and recrystallized quartz and are not correlated with growth of new quartz crystals.

We used a FE-SEM to image the recrystallized regions shown in Fig. 5. Acicular rutile crystals were not readily

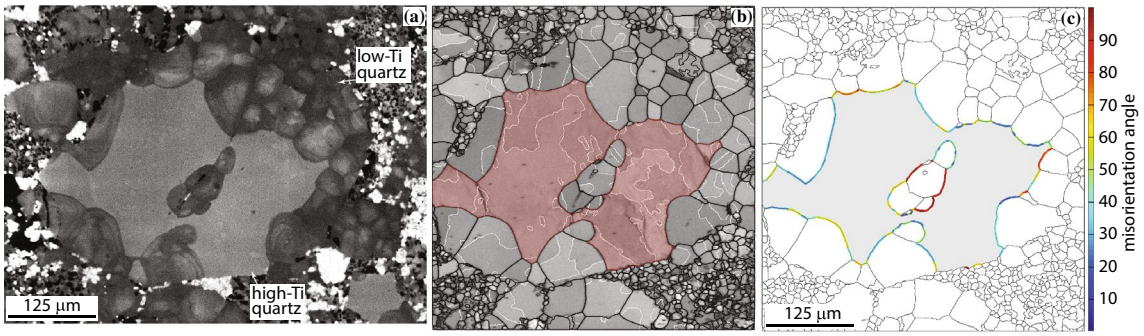

Fig. 5 Relict crystals of high-Ti quartz from a recrystallization experiment performed at 15 kbar and 925 °C (TiiGrB-20; Table 1) partially replaced by multiple smaller recrystallized grains. **a** Cathodoluminescence image showing a high-Ti quartz crystal with bright-CL that has smooth, cuspate boundaries surrounded by numerous smaller, equant low-Ti quartz crystals with dark-CL. **b** Band contrast electron backscatter diffraction map of a large, single crystal of high-Ti quartz (shaded in red) mantled with numerous smaller quartz crystals. White lines delineate Dauphiné twin boundaries. **c** Electron backscatter diffraction grain-boundary map with relict-recrystallized boundaries colorized by misorientation angle. Fine-grained minerals are mostly zircon and rutile. Scales in (**b**) and (**c**) are the same

visible in backscattered electron images collected using 5–10 kV accelerating voltages. We found that operating the FE-SEM at 20 kV increased the analytical volume and improved the chances of observing small rutile crystals, most of which were not exposed on the polished surfaces of specimens. Measurements of rutile crystals on backscattered electron images show that rutile crystals range from ~ 100 to 750 nm wide (Fig. 6a–d). Energy-dispersive spectroscopic analyses (Fig. 6e) agree with Raman analyses (Fig. 2) to confirm that acicular inclusions are rutile.

Discussion

Phenomenology

Low-Ti quartz included with numerous acicular rutile crystals discontinuously precipitated behind moving grain boundaries that advanced through high-Ti quartz starting material. Interfaces between the new and old quartz are sharp compositional and structural discontinuities (Figs. 3,4,5) that must have formed by grain-boundary migration. Based on the lack of acicular rutile crystals in the quartz starting material and abundant acicular rutile crystals in the new quartz, the Ti source for acicular rutile precipitation is likely from the decomposed high-Ti quartz starting material. The basic steps involved with the DP reaction,

$$\text{high-Ti quartz} = \text{low-Ti quartz} + \text{rutile}, \quad (2)$$

include structural decomposition of the high-Ti quartz starting material, formation of a new grain boundary, partitioning of Ti into the grain boundary, precipitation of rutile, and low-Ti quartz, followed by migration of the grain boundary. Figure 6c shows small rutile needles nucleated at a migrating grain boundary between low- and high-Ti quartz. Grain boundaries may sweep through materials numerous times to reduce system free energy because the first pass may not achieve textural and/or chemical equilibrium (Hay and Evans 1987; Yoon 1995; Manna et al. 2001; Evans et al. 2001). Given time, additional grain-boundary migration and DP may occur to reduce chemical zoning noted in the low-Ti quartz crystals (Figs. 4, 5). Changes to system *P–T–X* conditions may drive the discontinuous reaction described by Eq. 2 toward the left to cause discontinuous dissolution (Manna et al. 2001).

Energetics of discontinuous precipitation of quartz and rutile

These experiments provide information on the driving forces for DP in quartzites. Rutilated quartz formation in these experiments required the two independent events of initiation and steady-state growth of DP. Williams and Butler (1981) described the Gibbs energy change for initiation of DP as

$$\Delta G_I = \Delta G_p + \Delta G_{GB} + \Delta G_d + \Delta G_\epsilon \quad (3)$$

where subscripts p, GB, d, and ϵ terms refer to energy contributions from "puckering" and grain-boundary deflection near precipitate nuclei, grain boundary (related to grain shape and size), deformation (related to stored strain energy in the form of lattice dislocations), and compositional strain (related to changes in unit cell dimensions resulting from substitutional impurities). Energetics related to "puckering" and grain coarsening in quartzites are not fully understood. Energetics related to deformation are not relevant to the isostatic experiments described here (Nachlas et al. 2018a, b). Below, we consider the effect of compositional-related strain on DP.

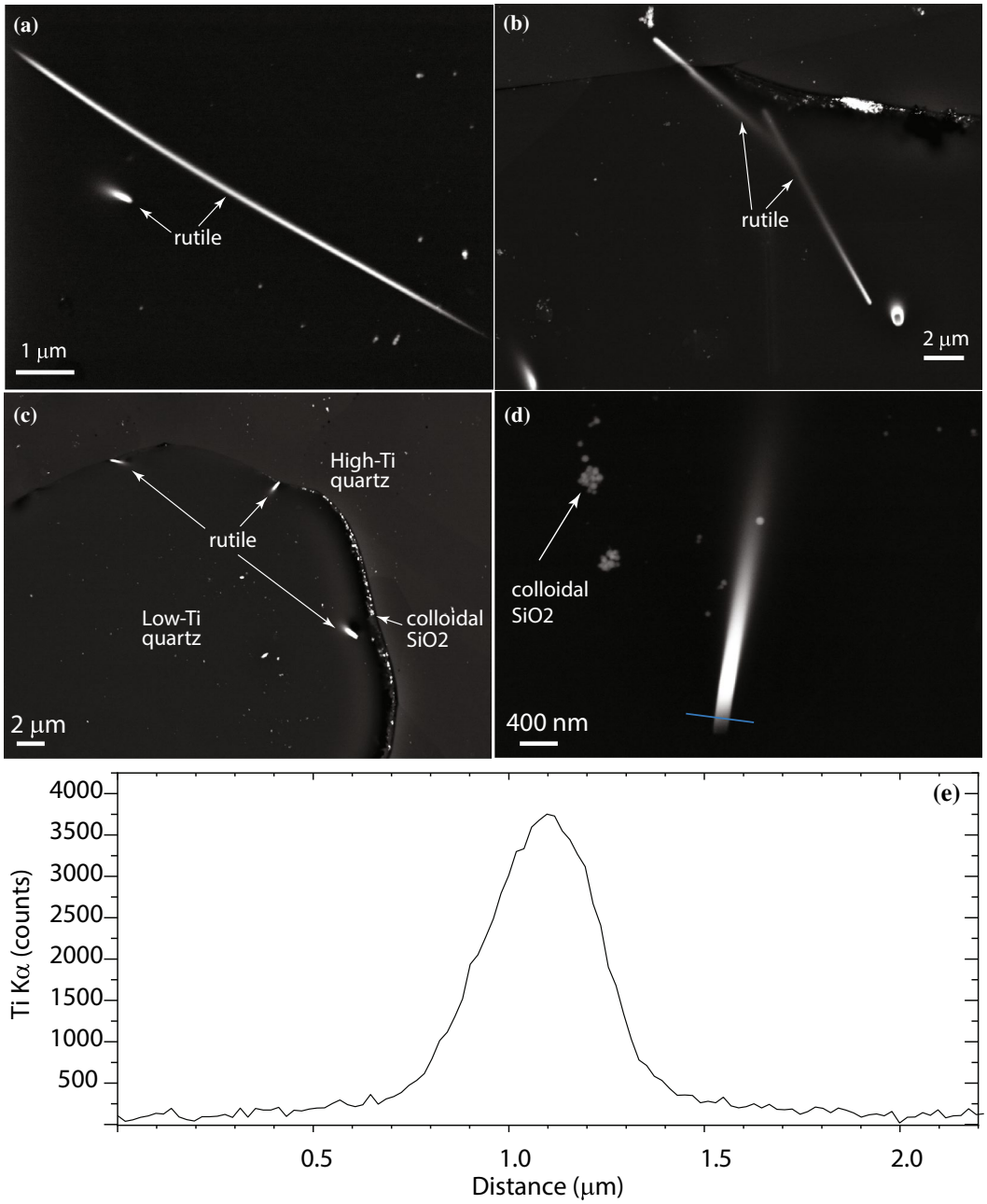

Fig. 6 Backscattered electron images (**a**–**d**) of rutilated quartz from recrystallization experiment performed at 15 kbar and 925 °C (Tii-GrB-20; Table 1), and **e** energy-dispersive spectrum showing Ti Kα X-rays obtained from a traverse (blue colored line) across the rutile crystal in **d**. Many rutile crystals intersect the polished surfaces at low angles which causes diffuse appearances to subsurface portions of the crystals. In **c** rutile needles are growing behind the low-Ti grain boundary that was advancing into the high-Ti quartz. The colloidal SiO_2 in dilated grain boundaries and on polished surfaces is from the polishing compound

After exceeding ΔG_I, the Gibbs energy change in DP for steady-state growth of DP minerals is

$$\Delta G_{DP} = \Delta G^{\gamma}_{DP} + \Delta G^{c}_{DP}, \quad (4)$$

where superscripts γ and c are the interfacial energy and chemical free energy (Williams and Butler 1981). We did not control surface areas of these experiments (e.g., grain size of starting material), but interfacial energetic contributions are believed to be small because quartz has a relatively low interfacial energy (~ 0.36 J/m^2) (Parks 1984). Results from the null recrystallization experiment performed at the synthesis condition (10 kbar and 925 °C) showed that annealing quartz starting material at a condition of chemical

equilibrium did not cause significant changes to microstructure, quartz Ti concentrations were not affected, and acicular rutile crystals did not form (Fig. 3a). This finding indicates that ΔG_d, ΔG_{GB} and ΔG_{DP}^{γ} are not sufficient to initiate and maintain steady-state DP in these experiments. Conversely, experimental results show that it is energetically favorable to initiate and grow new quartz and rutile crystals when the Ti concentrations of quartz deviate from the equilibrium solubility concentration by amounts characterized as trace element concentrations (< 0.1% by weight), which indicates that ΔG_{DP}^{c} is the dominant driving force for DP in these experimental quartzites (i.e., $\Delta G_{DP}^{c} \approx \Delta G_{DP}$).

The Ti concentration of the quartz starting material and the Ti-in-quartz solubility model of Thomas et al. (2010) can be used to calculate the Gibbs energy change (i.e., ΔG_{DP})—the 'driving force'—responsible for causing DP. Recrystallization experiments used quartz starting material with 376 ppm Ti (i.e., $lnX_{TiO_2}^{quartz} = -7.66$). In the null experiment where the starting material was recrystallized at the same condition at which it was synthesized (10 kbar and 925 °C), the Ti-in-quartz solubility model of Thomas et al. can be used to calculate that

$$\Delta G_{DP} = \frac{60.95\text{kJ}}{\text{mol}} - \left(1198K \bullet \frac{0.00152\text{kJ}}{\text{mol}K}\right) + \left(10\text{kbar} \bullet \frac{1.74\text{kJ}}{\text{kbar}}\right) + \left(\frac{0.008314\text{kJ}}{\text{mol}K} \bullet 1198K \bullet -7.66\right) \approx 0 \quad (5)$$

because the quartz remained in equilibrium (the model predicts perfect equilibrium for quartz with 367 ppm Ti = $lnX_{\text{TiO}_2}^{\text{quartz}} = -7.68$; Table 1). At 15, 20 and 25 kbar along the 925 °C isotherm the calculated equilibrium solubility concentrations of Ti in quartz are 153, 64 and 27 ppm Ti, respectively (Fig. 1). Changing the pressure value in the third term to 15, 20 and 25 kbar to represent conditions of the recrystallization experiments using quartz starting material with 367 ppm Ti (actual value measured was 376 ppm), gives ΔG_{DP} values of 8.7, 17.4 and 26.1 kJ/mol available to drive quartz recrystallization by DP. It is remarkable that compositional differences as small as ~ 0.03 wt% TiO_2 (~ 200 ppm Ti) were sufficient to drive extensive recrystallization of the synthetic quartzites. Even though DP was driven by trace element concentrations, it is important to emphasize that recrystallization experimental conditions imposed > 58% changes to the equilibrium solubility concentration of Ti in quartz. We performed experiments at 5 kbar increments in order to directly compare measured/predicted Ti-in-quartz concentrations with previous data (Thomas et al. 2010, 2015), but DP likely operates at even smaller concentration differences (i.e., smaller ΔG).

Compositional strain between neighboring grains in a polycrystalline material in which the crystals contain impurities could affect initiation and maintenance of grain-boundary migration (Yoon 1995). Strain may develop in quartz that has Ti concentrations that exceed the solubility limit for the imposed recrystallization experimental conditions. Ostapenko et al. (1987) measured unit-cell parameters of quartz that contained 0 to 1974 ppm Ti at room conditions. According to Ostapenko et al.'s unit-cell parameter data for Ti-bearing quartz, running the 367 ppm Ti quartz starting material at the recrystallization *P–T* condition at which the equilibrium solubility concentration was 153, 64, and 27 ppm, Ti would have caused strains of $+2.1\times10^{-5}$, $+3.0\times10^{-5}$, and $+3.4\times10^{-5}$ for the a-axis, and $+2.4\times10^{-5}$, $+3.3\times10^{-5}$, and $+3.8\times10^{-5}$ for the c-axis (positive strain values indicate an increase in unit cell dimension caused by Ti incorporation). The effect of pressure on unit-cell parameters of Ti-bearing quartz is unknown, and there are not yet any investigations on the nature of unmixing of high-Ti quartz into low-Ti quartz + acicular rutile, associated strain, and its effect on lattice coherency. It is plausible that reported elastic anisotropy caused by adding Ti to the quartz structure may affect nucleation of DP.

Grain-boundary migration rates

High-Ti quartz starting material recrystallized to form rocks with equilibrium microstructures and relatively uniform grain sizes. Textural evidence indicates that single crystals of quartz starting material were replaced by numerous, smaller crystals of recrystallized quartz (Fig. 5). We used average recrystallized grain sizes determined by the intercept method with known experimental durations (Table 1) to calculate the velocities of grain-boundary migration associated with DP.

To determine the number of grains intercepted, we drew 114 randomly oriented lines on CL and BSE images across regions that contained only newly recrystallized quartz. The lines of variable lengths intercepted 731 recrystallized quartz crystals to give an average grain size of 57 ± 1.1 μm (errors are estimated 2σ). The average grain sizes of all recrystallization experiments at P > 10 kbar are similar (Table 1), perhaps because recrystallization experiments were run for the same duration along an isotherm (i.e., 5 days at 925 °C), and recrystallization likely occurred via the same mechanism. Crystal growth rate was calculated by varying the volume of quartz added to growing crystals required to produce the average crystal sizes observed on CL, BSE, and EBSD images. For crystal growth rate calculations, we assumed that quasi-hexagonal-shaped grains are spherical, growth rate was constant throughout the 5-day experiments, and that nucleation of new crystals occurred instantaneously at a point source. Addition of 1.27×10^{-14} cm^3/s of quartz on an infinitesimally small nucleus during a 5-day experiment will produce crystals 5.53×10^{-9} cm^3 with 2-D radii of 28.5 μm

observed in cross-section. Interestingly, the growth rates of recrystallized grains from all recrystallization experiments are similar even though *G* varies by a factor of three.

In nominally dry systems, processes including DP, volume diffusion, and grain-boundary diffusion, can modify the Ti concentration of quartz. These experiments demonstrate that DP operates significantly faster than other mass transfer mechanisms. Consider an example using the above crystal growth rates caused by DP at 925 °C, a 100-µm diameter sphere of quartz with 200 ppm Ti recrystallized at a condition at which the equilibrium solubility is 100 ppm Ti. The crystal would relinquish all of its excess Ti in 27 days leaving behind new acicular rutile crystals and quartz crystals with the equilibrium solubility concentration of Ti. Diffusion of Ti in quartz grain boundaries (Bromiley and Hiscock 2016) is significantly faster than volume diffusion of Ti through the quartz structure (Cherniak et al. 2007). Grain-boundary diffusion can deliver Ti toward or away from the surface of a quartz crystal in a quartzose rock, but volume diffusion is required to change the Ti concentration of the interior of a crystal. The occurrence of rutilated quartz indicates that grain-boundary migration outpaced the capability of grain-boundary diffusion to transport Ti to preexisting rutile grains from the starting materials that reside on grain-boundaries (Fig. 4b–d). For the above example, volume diffusion would cause a concentration gradient in only the outer ~ 2 µm of the aforementioned 100-µm-diameter sphere to produce a fractional loss of ~ 3% of its Ti.

Evidence for discontinuous precipitation in natural quartz-rich rocks

Discontinuous precipitation is so efficient at changing the Ti concentrations of quartz that the only trace it may leave behind after protracted metamorphic events may be dark-CL quartz with numerous randomly oriented rutile crystals and/or dark-CL quartz consuming bright quartz with cuspate grain boundaries. There are several reported occurrences of DP in quartzites characterized by weak oscillatory zoning of low-Ti quartz consuming high-Ti quartz. Müller et al. (2007) documented kyanite quartzites with dark-CL quartz consuming bright-CL quartz with cuspate grain boundaries in a kyanite quartzite from Tverrådalen, Norway. They speculated that high-purity quartzites were produced through DP-type processes described above.

Quartz-rich migmatites at Fall Mountain near Bellows Fall, Vermont (USA) have CL textures (Spear and Wark 2009) strikingly similar to textures we interpret as resulting from DP (Fig. 7a, b). Based on chemical zoning, the dark-CL quartz with relatively low Ti concentrations (< 4–15 ppm) partially consumed the bright-CL quartz with higher Ti concentrations (13–32 ppm). Both types of quartz have Ti zoning, indicating some disequilibrium remains, and both types of quartz contain acicular rutile needles, which suggests that grain boundaries may have previously swept through the crystals during the approach to chemical equilibrium. The rocks exhibit CL textures in which low-Ti quartz was apparently consuming high-Ti quartz to produce an equilibrium microstructure characterized by ~ 120° triple junctions between crystals (Fig. 7c, d).

Previously described mechanisms to form rutilated quartz do not reflect DP phenomenology described above. A complete discussion of rutilated quartz occurrences and quartz with other types of acicular mineral inclusions is beyond the scope of this paper, but we provide a brief overview for comparative purposes. Two generalized mechanisms to form quartz with acicular inclusions are entrapment of preexisting acicular crystals by growing quartz, and unmixing (exsolution) of high-Ti quartz into low-Ti quartz and acicular rutile.

An entrapment mechanism is most likely for incorporating multi-component acicular minerals as inclusions because most other common inclusion minerals (e.g., ilmenite) are composed of elements with sufficiently low solubilities in the quartz structure that an external source is required (Sorby and Butler 1869; Ma et al. 2002; Seifert et al. 2011; Deer et al. 2013). The blue coloration of quartz in igneous rocks is commonly attributed to the occurrence of numerous acicular inclusions. Seifert et al. (2011) determined that sub-micrometer acicular crystals of mica and ilmenite are more abundant than rutile in some igneous blue quartzes. They suggested inclusion dimensions cause blue coloration of some quartz. Because most essential constituent elements of micas and ilmenite (e.g., Fe, Mg) do not have sufficiently high solubilities in the quartz structure, the inclusion minerals were interpreted to have grown from boundary layer melts adjacent to crystal-melt interfaces that were saturated in elements excluded by growing quartz. Sub-micrometer crystals nucleated in boundary layer regions were subsequently entrapped by growing quartz crystals.

Medium- to high-grade metamorphic rocks commonly have quartz with acicular rutile needles (Storm and Spear 2009; Adachi et al. 2010). In some cases, rutile needles (tetragonal crystal system) reportedly have preferred orientations coincident with the trigonal symmetry of the host quartz. Coincidence of crystallographic orientations has been interpreted as evidence that rutile homogeneously exsolved from quartz that initially contained high Ti concentrations (Jayaraman 1939; Herz and Force 1987; Adachi et al. 2010). Titanium-depleted halos in quartz surrounding rutile needles indicate that acicular rutile precipitation likely involved volume diffusion of Ti in the quartz structure (Wark and Watson 2006; Cherniak et al. 2007; Storm and Spear 2009; Nachlas et al. 2018b). Not all quartz with acicular rutile crystals show the evidence for diffusion-controlled rutile precipitation, and in most reported occurrences, rutile distribution is random,

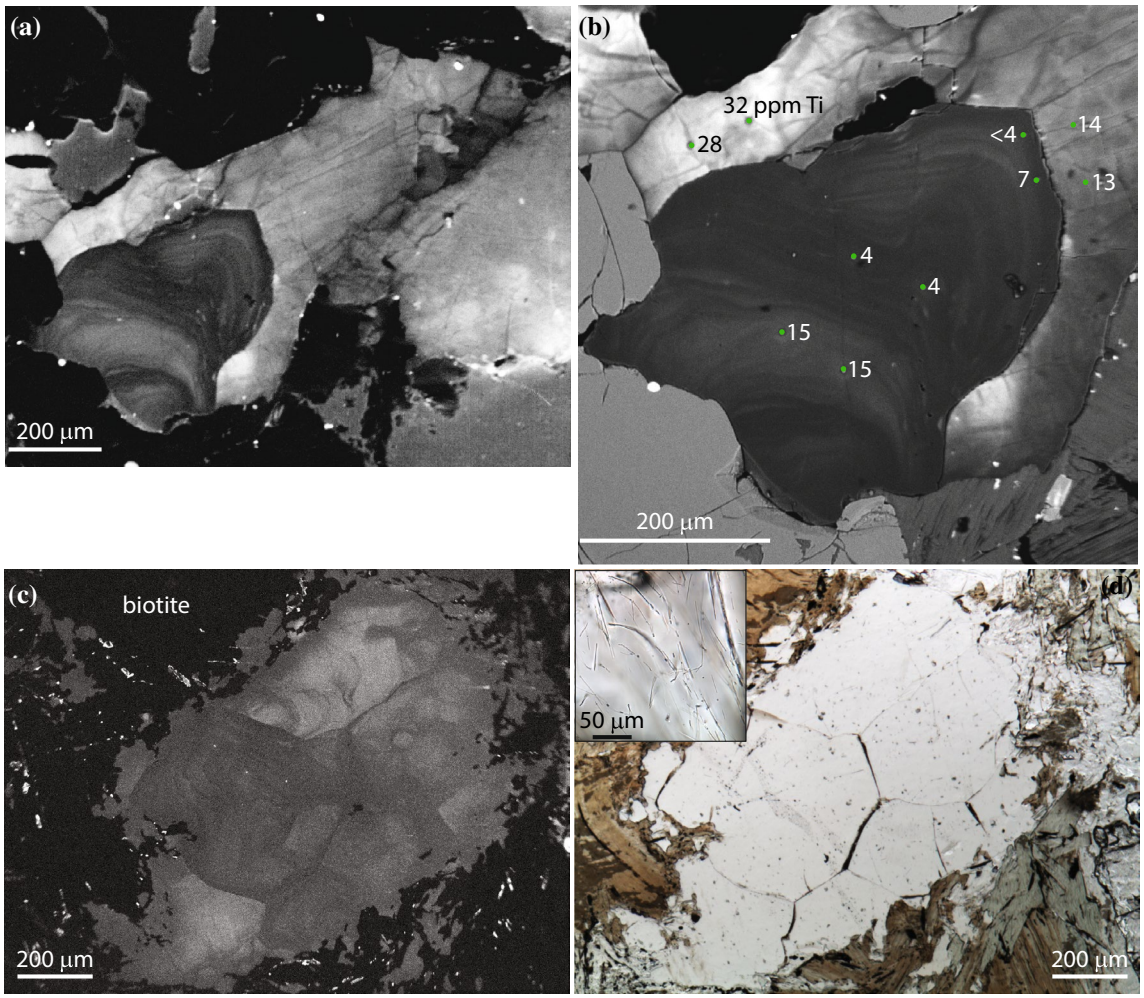

Fig. 7 Cathodoluminescence images and a light photomicrograph of migmatitic rocks at Fall Mountain near Bellows Falls, New Hampshire (USA). **a**, **b** Large crystal of dark-CL quartz with low Ti concentrations impinging on bright-CL quartz with higher Ti concentrations. Concentric zoning of quartz crystals suggests that some chemical disequilibrium remains. Cathodoluminescence image (**c**) and the corresponding transmitted plane-polarized light photomicrograph (**d**) showing weakly zoned, dark-CL quartz that contains acicular rutile crystals (inset) forming a microstructure with ~ 120° triple junctions surrounded by biotite and chlorite (lower right). The crystals and Ti concentrations (EPMA) shown in (**a**) and (**b**) are the same as those that appear in Spear and Wark (2009)

both of which suggest operation of alternative rutilation mechanisms such as discontinuous precipitation.

Implications

The identification of trace-level compositional driving forces for initiating grain-boundary migration has significant implications for the geochemistry and petrology of the associated minerals, the resultant microstructure of the rocks, and mineral fabrics that are used for geophysical interpretation of seismic anisotropy in the deep crust.

Quartz, rutile, and zircon geochemistry is commonly used for petrogenetic interpretations. Equilibrium solubility models for Ti in quartz, Ti in zircon, and Zr in rutile can be used to determine the crystallization *P*–*T* conditions, and rutile and zircon can be used for geochronology. The mechanism by which rutile inclusions in quartz form will affect their trace element and isotopic compositions, which has implications for thermobarometric applications that use *P*–*T* dependencies of Ti-in-quartz and Zr-in-rutile solubilities, and oxygen isotopic compositions of quartz-rutile pairs (Shulaker et al. 2015). For example, the acicular rutile needles in these experiments were likely not chemically equilibrated with zircon, which means that Zr-in-rutile measurements would not return the equilibrium solubility of Zr in rutile.

Discontinuous reactions can significantly change mineral compositions and, in the absence of a free fluid phase, can operate much faster than other types of mass transfer

processes commonly associated with solid-state reactions. Changes to *P–T* conditions during cooling, exhumation, and subsequent metamorphic events must change equilibrium concentration of Ti in quartz, which in turn can induce discontinuous reactions to accommodate changes to trace element solubilities in minerals. Titanium and Al typically have the highest concentrations of all impurities in quartz. Because Al concentrations of quartz vary systematically with pressure and temperature (Nachlas and Thomas 2018), imposed changes to *P–T* conditions that reduce the equilibrium solubility concentration of Al in quartz will likely cause DP and simultaneous precipitation of an aluminosilicate mineral.

Textural differences between the water-saturated experiments of Thomas et al. (2015) and the nominally dry experiments described here can be used to infer relative rates of crystal growth and grain-boundary transport. The water-saturated experiments did not contain acicular rutile crystals, which implies that excess Ti was partitioned into the grain-boundary fluid and advected away from the moving grain boundary, likely to preexisting granular rutile crystals residing along grain boundaries. Conversely, the presence of acicular rutile crystals in the nominally dry experiments described here implies that excess Ti partitioned into grain boundaries nucleated acicular rutile needles, which means that grain-boundary diffusion was not sufficient to transport excess Ti away from moving grain boundaries. The presence of randomly oriented acicular rutile crystals in quartz may provide indirect evidence for metamorphism under anhydrous conditions.

We induced DP by imposing chemical disequilibrium of ~ 200 ppm Ti, but smaller differences likely cause DP. Natural quartz crystals with CL and microstructural textures interpreted as evidence for DP (Fig. 7) imply that DP may be induced by changes to the equilibrium solubility of Ti in quartz at concentrations of less than ~ 10 ppm Ti. A change in pressure by ~ 1 kbar or a temperature change of ~ 20 °C can cause a change to the equilibrium solubility of Ti in quartz equivalent to ~ 10 ppm, which could cause microstructural changes. There is extensive evidence for operation of the related moving grain-boundary process of chemically induced grain-boundary migration in carbonates (Hay and Evans 1987; Evans et al. 2001; McCaig et al. 2007). We suggest that compositional modifications caused by moving grain boundaries can operate to rapidly change the chemical compositions of many other rock-forming minerals over short timescales. It is likely that discontinuous dissolution (Manna et al. 2001) may also play an important role in the formation of quartzite geochemistry and microstructural development.

Grain-boundary migration is arguably the most important grain-scale process for modifying the microstructure of rocks, and these results show that GBM driven by changes to mineral stability could modify rock microstructures under hydrostatic conditions. In earth materials, grain-boundary migration is typically associated with dislocation-accommodated deformation mechanisms and results in the formation of a mineral fabric reflecting the orientation of principal stresses imposed on the sample. Quartz grains in rocks that have been strongly deformed by plastic deformation mechanisms will retain a crystal-preferred orientation which, in combination with the seismic anisotropy exhibited by quartz single crystals, can be used to infer patterns of ductile flow in the lithosphere (Lowry and Pérez-Gussinyé 2011). However, recent evidence from experimental annealing of previously deformed samples has suggested that it may be possible to produce rock fabrics that do not reflect tectonic stresses (Boneh et al. 2017). Static annealing could act to reduce the intensity of a rock fabric and under certain conditions may even result in the formation of a secondary fabric with no relation to the stress experienced by the sample. As recrystallization acts to reduce the bulk free energy of the rock, low-energy boundary misorientations will form preferentially. Depending on the crystal system of the material in question, certain boundary misorientations have lower energy that correspond to the density of shared or coincident lattice sites (McLaren 1986). The results of these experiments indicate that changes to the equilibrium solubility at the trace element level can drive recrystallization to reduce system free energy. If grains are preferentially reorganized into specific low energy misorientations in response to changes in mineral compositional stability, it is possible to develop a rock fabric that does not reflect the external stress, a process that would complicate the interpretation of seismic anisotropy.

Numerous outstanding questions remain on how DP affects the chemistry and microstructure of rocks. The extent to which DP can affect the compositions of rocks may be revealed through experimental studies and detailed observations of natural samples. Temperature must affect grain-boundary velocities, but temperature dependence of DP in silicate minerals is unknown. Small fluctuations in *P* or *T* may cause grain boundaries to sweep through the same crystal more than once (Hay and Evans 1987; Manna et al. 2001; Evans et al. 2001; McCaig et al. 2007), and oscillating grain boundaries will certainly modify previously developed microstructures. We determined the rate of crystal growth in response to DP, but it is conceivable that grain-boundary velocities are not constant. Systematic studies may also reveal how the presence of additional minerals in the path of a migrating grain boundary affects grain-boundary velocities. Additionally, there are not yet sufficient data to evaluate the effects of grain misorientation on grain-boundary velocities. Acicular rutile crystals grew at the migrating grain boundaries on all faces of individual crystals, but there

may be crystallographic orientation relationships that control the distribution of rutile crystals along grain boundaries.

Acknowledgements This research was made possible through grants provided by the National Science Foundation to JBT. Most results were supported by EAR1551343; pilot experiments were performed with funds from EAR1543627. An MRI grant through the NSF Earth Sciences Division (EAR1625835) and support from Syracuse University provided electron microprobe facilities used for much of this research. The authors thank F. Spear for providing migmatite samples from New Hampshire. An anonymous reviewer greatly improved an earlier version of the manuscript.

References

Adachi T, Hokada T, Osanai Y et al (2010) Titanium behavior in quartz during retrograde hydration: occurrence of rutile exsolution and implications for metamorphic processes in the Sør Rondane Mountains, East Antarctica. Polar Sci 3:222–234. https://doi.org/10.1016/j.polar.2009.08.005

Bachmann F, Hielscher R, Schaeben H (2010) Texture analysis with MTEX—free and open source software toolbox. Solid State Phenom 160:63–68. https://doi.org/10.4028/www.scientific.net/SSP.160.63

Boland JN, Otten MT (1985) Symplectitic augite; evidence for discontinuous precipitation as an exsolution mechanism in Ca-rich clinopyroxene. J Metamorph Geol 3:13–20

Boland JN, van Roermund HLM (1983) Mechanisms of exsolution in omphacites from high temperature, type B, eclogites. Phys Chem Miner 9:30–37

Bonazzi M, Tumiati S, Thomas J et al (2019) Assessment of the reliability of elastic geobarometry with quartz inclusions. Lithos. https://doi.org/10.1016/j.lithos.2019.105201

Boneh Y, Wallis D, Hansen LN et al (2017) Oriented grain growth and modification of 'frozen anisotropy' in the lithospheric mantle. Earth Planet Sci Lett 474:368–374. https://doi.org/10.1016/j.epsl.2017.06.050

Bromiley GD, Hiscock M (2016) Grain boundary diffusion of titanium in polycrystalline quartz and its implications for titanium in quartz (TitaniQ) geothermobarometry. Geochim Cosmochim Acta 178:281–290. https://doi.org/10.1016/j.gca.2016.01.024

Cherniak DJ, Watson EB, Wark DA (2007) Ti diffusion in quartz. Chem Geol 236:65–74. https://doi.org/10.1016/j.chemgeo.2006.09.001

Deer WA, Howie RA, Zussman J (2013) An introduction to the rock-forming minerals, 3rd edn. The Minerological Society, London

Evans B, Renner J, Hirth G (2001) A few remarks on the kinetics of static grain growth in rocks. Int J Earth Sci 90:88–103. https://doi.org/10.1007/s005310000150

Farver JR, Yund RA (1992) Oxygen diffusion in a fine-grained quartz aggregate with wetted and nonwetted microstructures. J Geophys Res 97:14017. https://doi.org/10.1029/92JB01206

Hay RS, Evans B (1987) Chemically induced grain boundary migration in calcite: temperature dependence, phenomenology, and possible applications to geologic systems. Contrib Mineral Petrol 97:127–141. https://doi.org/10.1007/BF00375220

Herz N, Force ER (1987) Geology and mineral deposits of the Roseland District of central Virginia

Hiraga T, Anderson I, Zimmerman M et al (2002) Structure and chemistry of grain boundaries in deformed, olivine + basalt and partially molten lherzolite aggregates: evidence of melt-free grain boundaries. Contrib Mineral Petrol 144:163–175. https://doi.org/10.1007/s00410-002-0394-1

Hiraga T, Hirschmann MM, Kohlstedt DL (2007) Equilibrium interface segregation in the diopside–forsterite system II: applications of interface enrichment to mantle geochemistry. Geochim Cosmochim Acta 71:1281–1289. https://doi.org/10.1016/j.gca.2006.11.020

Hiraga T, Kohlstedt DL (2007) Equilibrium interface segregation in the diopside–forsterite system I: analytical techniques, thermodynamics, and segregation characteristics. Geochim Cosmochim Acta 71:1266–1280. https://doi.org/10.1016/j.gca.2006.11.019

Hirth G, Tullis J (1992) Dislocation creep regimes in quartz aggregates. J Struct Geol 14:145–159. https://doi.org/10.1016/0191-8141(92)90053-Y

Jayaraman N (1939) The cause of colour of the blue quartzes of the charnockites of south India and the Champion gneiss and other related rocks of mysore. Proc Indian Acad Sci Sect A 9:265–285. https://doi.org/10.1007/BF03046467

Lafuente B, Downs RT, Yang H, Stone N (2015) The power of databases: the RRUFF project. In: Armbruster T, Danisi RM (eds) Highlights in mineralogical crystallography. DE GRUYTER, Berlin, pp 1–30

Lowry AR, Pérez-Gussinyé M (2011) The role of crustal quartz in controlling Cordilleran deformation. Nature 471:353–357. https://doi.org/10.1038/nature09912

Ma C, Goreva JS, Rossman GR (2002) Fibrous nanoinclusions in massive rose quartz: HRTEM and AEM investigations. Am Mineral 87:269–276. https://doi.org/10.2138/am-2002-2-308

Manna I, Pabi SK, Gust W (2001) Discontinuous reactions in solids. Int Mater Rev 46:53–91. https://doi.org/10.1179/095066001101528402

McCaig A, Covey-Crump SJ, Ben Ismaïl W, Lloyd GE (2007) Fast diffusion along mobile grain boundaries in calcite. Contrib Mineral Petrol 153:159–175. https://doi.org/10.1007/s00410-006-0138-8

McLaren AC (1986) Some speculations on the nature of high-angle grain boundaries in quartz rocks. In: Hobbs BE, Heard HC (eds) Geophysical monograph series. American Geophysical Union, Washington, D. C., pp 233–245

Müller A, Ihlen PM, Wanvik JE, Flem B (2007) High-purity quartz mineralisation in kyanite quartzites, Norway. Miner Depos 42:523–535. https://doi.org/10.1007/s00126-007-0124-8

Nachlas WO, Thomas JB (2018) Aluminum solubility in quartz and application of the single mineral crossing isopleths method. GSA Annu Meet Indianapolis, Indiana

Nachlas WO, Thomas JB, Hirth G (2018a) TitaniQ deformed: Experimental deformation of out-of-equilibrium quartz porphyroclasts. J Struct Geol 116:207–222. https://doi.org/10.1016/j.jsg.2018.07.012

Nachlas WO, Teyssier C, Whitney DL, Hirth G (2018b) Diffusion geospeedometry in natural and experimental shear zones. Earth Planet Sci Lett 498:129–139. https://doi.org/10.1016/j.epsl.2018.06.025

Nichols CIO, Krakow R, Herrero Albillos J et al (2018) Microstructural and paleomagnetic insight into the cooling history of the IAB parent body. Geochim Cosmochim Acta 229:1–19. https://doi.org/10.1016/j.gca.2018.03.009

Ostapenko GT, Gamarnik MY, Gorogotskaya LI et al (1987) Isomorphism of Titanium Substitution for Silicon in Quartz: Experimental Data. Mineral Zhurnal 9:30–40

Parks GA (1984) Surface and interfacial free energies of quartz. J Geophys Res Solid Earth 89:3997–4008. https://doi.org/10.1029/JB089iB06p03997

Putnis A (1992) Introduction to mineral sciences. Cambridge University Press, Cambridge

Seifert W, Rhede D, Thomas R et al (2011) Distinctive properties of rock-forming blue quartz: inferences from a multi-analytical study of submicron mineral inclusions. Mineral Mag 75:2519–2534. https://doi.org/10.1180/minmag.2011.075.4.2519

Shigematsu N, Prior DJ, Wheeler J (2006) First combined electron backscatter diffraction and transmission electron microscopy study of grain boundary structure of deformed quartzite. J Microsc 224:306–321. https://doi.org/10.1111/j.1365-2818.2006.01697.x

Shulaker DZ, Schmitt AK, Zack T, Bindeman I (2015) In-situ oxygen isotope and trace element geothermometry of rutilated quartz from Alpine fissures. Am Mineral 100:915–925. https://doi.org/10.2138/am-2015-4961

Sorby HC, Butler PJ (1869) On the structure of rubies, sapphires, diamonds, and some other minerals. Proc R Soc Lond 17:291–302. https://doi.org/10.1098/rspl.1868.0050

Spear FS, Ashley KT, Webb LE, Thomas JB (2012) Ti diffusion in quartz inclusions: implications for metamorphic time scales. Contrib Mineral Petrol 164:977–986. https://doi.org/10.1007/s00410-012-0783-z

Spear FS, Thomas JB, Hallett BW (2014) Overstepping the garnet isograd: a comparison of QuiG barometry and thermodynamic modeling. Contrib Mineral Petrol. https://doi.org/10.1007/s00410-014-1059-6

Spear FS, Wark DA (2009) Cathodoluminescence imaging and titanium thermometry in metamorphic quartz. J Metamorph Geol 27:187–205. https://doi.org/10.1111/j.1525-1314.2009.00813.x

Storm LC, Spear FS (2009) Application of the titanium-in-quartz thermometer to pelitic migmatites from the Adirondack Highlands, New York. J Metamorph Geol 27:479–494. https://doi.org/10.1111/j.1525-1314.2009.00829.x

Teng F-Z, McDonough WF, Rudnick RL, Walker RJ (2006) Diffusion-driven extreme lithium isotopic fractionation in country rocks of the Tin Mountain pegmatite. Earth Planet Sci Lett 243:701–710. https://doi.org/10.1016/j.epsl.2006.01.036

Thomas JB, Spear FS (2018) Experimental study of quartz inclusions in garnet at pressures up to 3.0 GPa: evaluating validity of the quartz-in-garnet inclusion elastic thermobarometer. Contrib Mineral Petrol. https://doi.org/10.1007/s00410-018-1469-y

Thomas JB, Watson EB (2014) Diffusion and partitioning of magnesium in quartz grain boundaries. Contrib Mineral Petrol 168:1–12. https://doi.org/10.1007/s00410-014-1068-5

Thomas JB, Watson EB, Spear FS et al (2010) TitaniQ under pressure: the effect of pressure and temperature on the solubility of Ti in quartz. Contrib Mineral Petrol 160:743–759. https://doi.org/10.1007/s00410-010-0505-3

Thomas JB, Watson EB, Spear FS, Wark DA (2015) TitaniQ recrystallized: experimental confirmation of the original Ti-in-quartz calibrations. Contrib Mineral Petrol 169:1–16. https://doi.org/10.1007/s00410-015-1120-0

Tominaga A, Kato T, Kubo T, Kurosawa M (2009) Preliminary analysis on the mobility of trace incompatible elements during the basalt and peridotite reaction under uppermost mantle conditions. Phys Earth Planet Int 174:50–59. https://doi.org/10.1016/j.pepi.2008.09.019

Urai JL, Means WD, Lister GS (1986) Dynamic recrystallization of minerals. In: Hobbs BE, Heard HC (eds) Geophysical monograph series. American Geophysical Union, Washington, D. C., pp 161–199

Wark DA, Watson EB (2006) TitaniQ: a titanium-in-quartz geothermometer. Contrib Mineral Petrol 152:743–754. https://doi.org/10.1007/s00410-006-0132-1

Watson E, Wark D, Price J, Van Orman J (2002) Mapping the thermal structure of solid-media pressure assemblies. Contrib Mineral Petrol 142:640–652. https://doi.org/10.1007/s00410-001-0327-4

Williams DB, Butler EP (1981) Grain boundary discontinuous precipitation reactions. Int Met Rev 26:153–183. https://doi.org/10.1179/imtr.1981.26.1.153

Yoon DY (1995) Theories and observations of chemically induced interface migration. Int Mater Rev 40:149–179. https://doi.org/10.1179/imr.1995.40.4.149